In Situ Photolysis of CD_3I in Solid Orthodeuterium†

Mizuho Fushitani,‡,§ Yuki Miyamoto,‡ Hiromichi Hoshina,‡,|| and Takamasa Momose*,‡,⊥

Department of Chemistry, Graduate School of Science, Kyoto University, Kyoto 606-8502, Japan, and Department of Chemistry, The University of British Columbia, 2036 Main Mall, Vancouver BC, V6T1Z1, Canada

Received: July 31, 2007; In Final Form: October 12, 2007

Photochemical reactions of molecules in solid orthodeuterium (o-D_2) have been studied by high-resolution infrared spectroscopy and compared with previous results obtained in solid parahydrogen (p-H_2). Ultraviolet photolysis of CD_3I molecules in solid o-D_2 yielded CD_3 radicals and iodine atoms efficiently, which indicates a small cage effect in solid o-D_2, as in the case of solid p-H_2. The Fourier transform infrared spectrum of the ν_3 vibrational band of CD_3 showed a rotational structure with additional splitting due to crystal field interactions. The magnetic dipole transition ($^2P_{1/2} \leftarrow {}^2P_{3/2}$) of the I atom isolated in solid o-D_2 was observed together with a strong rotational satellite of deuterium molecules through the electron−roton coupling in solid hydrogen. The tunneling reaction between CD_3 and D_2 was not observed in a time scale of a few days, which gives the upper limit of the tunneling reaction rate of 10^{-8} s^{-1} at 4.2 K.

Introduction

Quantum matrices such as solid parahydrogen (p-H_2)[1−8] and superfluid He droplets[9−13] are proven to be excellent matrices for high-resolution spectroscopy of cold molecules. Molecules embedded in these quantum matrices exhibit quantized rotational states and extremely long lifetime of vibration−rotation excited states, which makes the rovibrational transitions of molecules in these quantum matrices extremely narrow. The spectral linewidths are narrow enough to resolve fine spectral structures originated in subtle interaction between guest and host molecules/atoms.

It has also been proven that these quantum matrices are applied to the study of chemical reactions at low temperatures.[3,12,13] Due to the weak cage effect, molecules in these quantum matrices can be easily dissociated by photons, and radicals produced by the photolysis are subjected to further reactions at low temperatures. Especially, solid p-H_2 is useful for the study of low-temperature reactions, such as quantum tunneling reactions,[3,14,15] which are supposed to be very slow.

It has been demonstrated[16−18] that in situ photolysis of alkyl iodides in solid p-H_2 yields the alkyl radicals and I atoms, which is in contrast with rare gas matrices, where in situ photolysis does not result in dissociation due to recombination caused by the strong cage effect.[19−22] Recently, it has been shown that chlorine molecules can be dissociated in solid p-H_2 by UV photons as well.[6,23] The production of radicals and atoms in solid p-H_2 allowed us to study various reactions and low-temperature dynamics. They include quantum diffusion of H atoms,[24,25] chemical reactions via tunneling effect,[14,15] infrared induced chemical reaction,[6,26] and nuclear spin conservation in chemical reactions.[27,28]

The advantage of solid p-H_2 stems from the weak intermolecular interactions in solid p-H_2 and the softness of quantum crystal. Parahydrogen molecules at liquid He temperatures occupy the $J = 0$ rotational state with the $I = 0$ nuclear spin state only. Since the $J = 0$ rotational wavefunction is spherical, p-H_2 molecules possess no permanent multipole moments of any order as an average, so that intermolecular interaction in solid p-H_2 is essentially weak. Another important feature of solid p-H_2 is its quantum nature due to the small mass of H_2. Solid p-H_2 is classified as a quantum crystal. One of the characteristics of quantum crystals is its large amplitude of zero-point lattice vibration (ZPLV). In the case of solid p-H_2, the amplitude extends more than 1.5 Å.[29] The large amplitude makes the intermolecular distance between two H_2 molecules in solid p-H_2 very large, that is, 3.8 Å.[30,31] Note that the minimum of the pair potential between two H_2 molecules is 3.2 Å, which is significantly smaller than the intermolecular distance in solid p-H_2. As a result of the large intermolecular distance, interactions in solid p-H_2 become extremely weak. In addition, the large ZPLV makes solid p-H_2 soft, which is the origin of the small cage effect observed in solid p-H_2.

Solid deuterium (D_2) is also regarded as a quantum crystal; therefore, it is expected to have features as a matrix similar to those of solid p-H_2.[29−31] Because of the $I = 1$ nuclear spin of the deuterium atom, there are three nuclear spin modifications of deuterium molecules, that is, $I = 0$, 1, and 2. Due to the symmetry restriction of the rotational and nuclear spin wave functions of D_2, rotational states with *even* quantum numbers are coupled with the $I = 0$ and $I = 2$ nuclear spin states, while rotational states with *odd* numbers are coupled with the $I = 1$ nuclear spin state. The former is called orthodeuterium (o-D_2), and the latter is called paradeuterium (p-D_2). The statistical ratio between o-D_2 and p-D_2 is 2:1. Because of the large rotational constant ($B = 30$ cm^{-1})[29] of D_2, o-D_2 occupies only the $J = 0$ rotational state and p-D_2 the $J = 1$ state at liquid He temperatures. Therefore, o-D_2 at liquid He temperatures has no permanent multipole moments other than weak magnetic

† Part of the "Giacinto Scoles Festschrift".

* To whom correspondence should be addressed. Electronic mail: momose@chem.ubc.ca.

‡ Kyoto University.

§ Present address: Institute for Molecular Science, Okazaki, Japan.

|| Present address: Terahertz Sensing and Imaging Laboratory, RIKEN, Sendai, Japan.

⊥ The University of British Columbia.

10.1021/jp0761113 CCC: $37.00
Published on Web 11/13/2007

moments induced by the $I = 2$ spin state. As a result, interaction in solid o-D_2 is expected to be very small, as in the case of solid p-H_2.

The effective quantum de Boer parameters[32] of solid p-H_2, solid o-D_2, and solid Ne are 1.731, 1.224, and 0.58, respectively.[31] The quantum parameter is a dimensionless parameter that defines the magnitude of the quantum mechanical effect in solids. The parameter is roughly proportional to the amplitude of ZPLV.[31] Since the quantum parameter of deuterium is still significantly larger than that of Ne, the ZPLV is expected to be relatively large in solid deuterium, which reduces the cage effect on photodissociation processes so that unstable species can be produced by in situ photolysis in solid o-D_2. Photochemistry of dopants in solid o-D_2 will provide us useful information on isotopic effects of chemical reactions at low temperatures, such as tunneling reactions.

So far, properties of solid o-D_2 itself have been investigated intensively,[33−38] while few spectroscopic studies on dopants in solid o-D_2 have been reported.[39−42] In the present paper, we have investigated in situ photolysis of CD_3I embedded in solid o-D_2 and compare these experiments with previous results obtained in solid p-H_2.

Experimental Section

With a help of magnetic catalysts kept at low temperatures, the concentration of o-D_2 can be increased as a result of the nuclear spin conversion from the $I = 1$ to either $I = 0$ or 2.[1,43] The ortho−para conversion normally takes place just above the melting point of hydrogen in order to maximize the contact between the magnetic catalysts and hydrogen at the lowest possible temperature. Since the melting point of solid D_2 is 18 K, the expected purity of o-D_2 is 98.8%, calculated from the thermal population between the $J = 0$ and $J = 1$ states at 18 K.[31] In our experiments, we converted n-D_2 into o-D_2 at 20 K using ferric oxide based ortho−para catalyst (IONEX-type). The equilibrium concentration of o-D_2 at this temperature is calculated to be 98.0%. We assume this o-D_2 concentration without any measurement.

Normal deuterium (99.93 atom %D, Cryogenic Rare Gas Inc.) with the ortho-to-para ratio of 2:1 was introduced into a stainless tube containing the ortho−para catalyst to make 98% of o-D_2 molecules, which was stored in a nonmagnetic vessel at the room temperature. The converted gas was mixed with CD_3I (>99 atom %D) with the concentration of 4−100 ppm. The premixed gas was sprayed onto a BaF_2 window kept at 4.2 K with the flow rate of ~50 cm^3 min^{-1}.[4] Crystals thus made were almost transparent, but slightly foggy due to some defects. All the spectroscopic measurements were done at 4.2 K.

Fourier transform infrared (FTIR) spectra with a resolution of 0.1 cm^{-1} were observed using an FTIR spectrometer (Bruker IFS 120HR) combined with a KBr or CaF_2 beam splitter and a liquid N_2 cooled MCT or InSb detector. UV pulses ($\lambda = 250$ nm, rep 10 Hz, 1−2 mJ/pulse) obtained as the second harmonics of visible pulses from a commercial OPO laser system (MOPO-SLX-W, Spectra Physics Inc.) pumped by a Nd:YAG laser (QUANTA-RAY PRO-230-10-W, Spectra Physics Inc.) were used for photolysis.

Results

Trace a in Figure 1 shows an FTIR spectrum of CD_3I isolated in solid o-D_2 as deposited, and trace b shows the spectrum after UV irradiation for 30 min. The concentration of CD_3I in the premixed gas was 4 ppm. Before the UV irradiation, absorption peaks of the ν_4 vibrational band of CD_3I were observed at 2150.4 and 2150.8 cm^{-1}. After the UV irradiation, the absorption bands of CD_3I at 2150.8 and 2150.4 cm^{-1} almost disappeared and new absorption bands were observed in the spectral regions of 2360−2410 and 7655 cm^{-1}. The former absorption is assigned to the ν_3 vibrational band of CD_3, referring to the gas-phase value of 2381 cm^{-1},[44] and the latter absorption to the magnetic dipole transition ($^2P_{1/2} \leftarrow {}^2P_{3/2}$) of I atoms, which appears at 7603 cm^{-1} in the gas phase.[45] The ultraviolet pulses at 250 nm dissociates the C−I bond of CD_3I molecules to yield CD_3 radicals and I atoms even in solid o-D_2. The formations of CD_3 radicals and I atoms indicate the small cage effect on the photodissociation in solid o-D_2. We note that the UV photon energy (~4.95 eV) amply exceeds the dissociation energy of the C−I bond (~2.3 eV), but no dissociation occurs in solid Ne,[19−22] while dissociation takes place in both solid p-H_2 and solid o-D_2. We do not have any quantitative data on how much the excess energy distributes to the internal and translational energies of the fragment radical, but the cage effect in solid hydrogen is weak enough so that the excess energy of 1−2 eV is enough for methyl radicals to be fragmented in these quantum crystals.

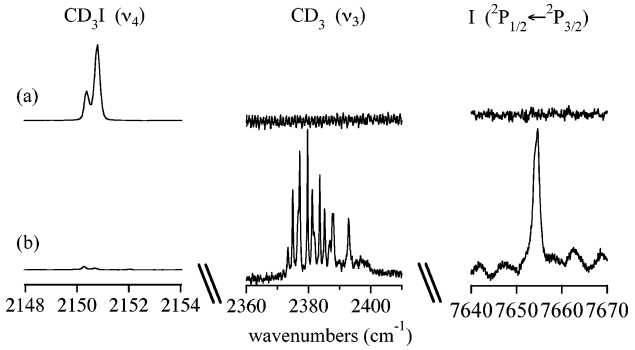

Figure 1. FTIR spectra of CD_3I in solid o-D_2 before and after the UV photolysis: (a) before UV irradiation and (b) after UV irradiation at 250 nm for 5 min. The assignments are given at the top of each transition.

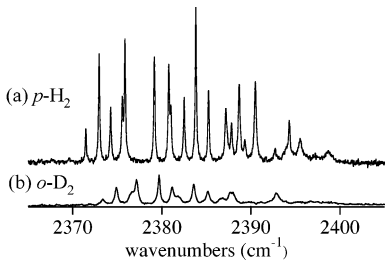

Figure 2. FTIR spectra of the ν_3 transition of CD_3 (a) in solid p-H_2 and (b) in solid o-D_2.

Discussion

(a) Rotational Structures. The ν_3 absorption band of CD_3 shows a rotational substructure with additional splittings caused by the crystal field potential.[2] The spectral structure is quite similar to that in solid p-H_2, as shown in Figure 2, indicating that CD_3 radicals in solid o-D_2 are rotating almost freely as in the case of those in solid p-H_2 and that the crystal structure around the CD_3 radical is hexagonal close packed, having D_{3h} point group symmetry.[46] The spectral structure shown in Figure 2 can be analyzed by the crystal field theory developed previously.[2,47] Details of the analysis will be published in a separate paper.[48] Here, we briefly describe the result of the analysis.

TABLE 1: Molecular Constants of CD_3 in Solid Hydrogen (in cm^{-1})

		solid *o*-D_2	solid *p*-H_2	gas[c]
rotational constant[a]	B	3.916	4.652	4.802
band origin[b]	ν_0	2379.71	2379.05	2381.09
Coriolis coupling	ζ	0.201 (fixed)	0.240	0.201
crystal field parameter	ϵ_2	0.16	0.30	-
crystal field parameter	ϵ_3	15.48	16.13	-

[a] The rotational constant in the ground vibrational state. The rotational constant *C* was fixed to 0.5*B*, by assuming that the radical has a planer structure with D_{3h} symmetry. [b] The band origin of the ν_3 transition. [c] References 44 and 51.

The Hamiltonian, *H*, we used for the analysis is expressed as a sum of the standard rotation−vibration Hamiltonian of the radical in free space, H_0,[49] and the anisotropic potential due to the electric field of surrounding lattice, V_{crys}, as

$$H = H_0 + V_{crys} \quad (1)$$

The crystal field is a function of the orientation of the radical, Ω, with respect to the crystal axes, and the explicit expression depends on the symmetry of the system. In the case of the methyl radical (D_{3h} point group) in a hexagonal close packed crystal (D_{3h} point group), it is given by[2]

$$V_{crys}(\Omega) = \epsilon_2 {D_{0,0}}^2(\Omega) + \epsilon_3[{D_{-3,-3}}^3(\Omega) - {D_{3,-3}}^3(\Omega) - {D_{-3,3}}^3(\Omega) + {D_{3,3}}^3(\Omega)] \quad (2)$$

where $D_{M,k}^{l}(\Omega)$ is Wigner rotation matrix,[50] and ϵ_i are coefficients. The anisotropy of the crystal field given in eq 2 lifts the degeneracy of the quantum number *M* of CD_3, where *M* is the projection of he rotational angular momentum with respect to the crystal axis. The splitting of the *M* level causes fine structures in vibration−rotation spectra seen in Figure 2. By using the least-squares fitting of the observed frequency, we could obtain rotational constants, Coriolis coupling constant, and the frequency of band origin as well as the crystal field parameters. Table 1 summarizes the molecular constants of CD_3 obtained from the analysis.

The frequency of the band origin of the ν_3 transition of CD_3 in solid *o*-D_2 is almost the same as that in solid *p*-H_2, and the shift from the gas-phase value is only 1−2 cm^{-1}. The small shift indicates that the perturbation of matrices to vibrational motion in solid *o*-D_2 is similar to that in solid *p*-H_2.

The rotational constant *B* of CD_3 in solid *o*-D_2 is about 82% of the gas-phase value, while that in solid *p*-H_2 is about 96%. The larger reduction of the rotational constants in solid *o*-D_2 than those in solid *p*-H_2 is partly due to the mass effect of the surrounding lattice.[52] The decrease of the rotational constants is a result of the increase of the effective moment of inertia, which is mainly caused by the motion of the surrounding hydrogen molecules in the lattice along with the rotation of CD_3. Such an analysis has been published in a previous paper for the case of methane.[2] The simple model[52] predicts that the increase of the moment of inertia is proportional to the mass of host molecules/atoms. Therefore, the increase of the moment of inertia in solid *o*-D_2 is expected to be twice of that in solid *p*-H_2. The observed larger reduction of the rotational constant in solid *o*-D_2 than that in solid *p*-H_2 can be explained by this model qualitatively. The observed increase of the moment of inertia, however, of CD_3 in solid *o*-D_2 with respect to the gas-phase value is about 5 times larger than that in solid *p*-H_2, which is more than the predicted ratio of 2 based on the simple model.[2,52] More detailed analysis is necessary to interpret the reduction of the rotational constants quantitatively.

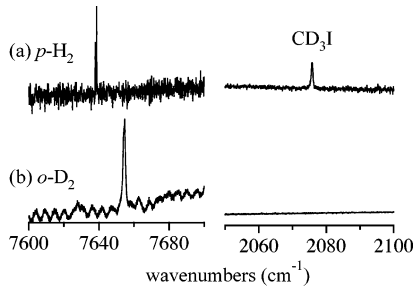

Figure 3. (a) An FTIR spectrum of the spin−orbit transition of I atoms in solid *p*-H_2. (b) An FTIR spectrum of the spin−orbit transition of I atoms in solid *o*-D_2. The concentration of CD_3I in the premixed gas was 4 ppm. The right panels show the corresponding spectral region of the absorption bands of CD_3I and C_2D_6.

TABLE 2: Observed Frequencies of the $^2P_{1/2} \leftarrow {}^2P_{3/2}$ Transition of I Atoms in Solid *o*-D_2 and *p*-H_2

	solid *o*-D_2	solid *p*-H_2
I (free)	7654.1, 7654.8	7637.8, 7638.5
I (complex)[a]	7674.2, 7674.9	7660.9, 7661.6
$I + S_0(0)$	7834[b]	7994[b]

[a] Complex with other neutral species such as CD_3I or C_2D_6. [b] Center frequency of the band.

The line width of CD_3 in solid *o*-D_2 is broader than that in solid *p*-H_2, as seen in Figure 2. The full-width at the half-maximum (fwhm) of the ν_3 absorption band of CD_3 in solid *o*-D_2 is about 0.4 cm^{-1}, while the fwhm in solid *p*-H_2 is about 0.2 cm^{-1}. The broader width in solid *o*-D_2 is due to the larger interaction in solid *o*-D_2 than in solid *p*-H_2, and possible inhomogeneities in the *o*-D_2 crystal structure. Another cause of the larger line width in solid *o*-D_2 is the larger concentration of $J = 1$ *p*-D_2 impurities than that of $J = 1$ *o*-H_2 impurities in solid *p*-H_2. The concentration of the residual $J = 1$ *p*-D_2 impurities in solid *o*-D_2 is about 2%, which is almost 40 times larger than that in solid *p*-H_2. It is known that the quadrupole moment of the $J = 1$ impurity in solid hydrogen causes significant broadening of line width due to electrostatic interaction.[53] If the $J = 1$ *p*-D_2 impurities exist next to the radicals, it should cause significant broadening in the spectrum of CD_3. It is possible that the electron spin of CD_3 could convert the nuclear spin of *p*-D_2 to *o*-D_2,[6] so that the lifetime of the $J = 1$ *p*-D_2 impurities next to the radical could be short. Since we did not observe any significant change in the line width upon annealing or after a few days, no experimental evidence on the nuclear spin conversion has been obtained on our experimental time scale. In any event, the broader line width could be a disadvantage of solid *o*-D_2 as a matrix host over solid *p*-H_2, but the width is still sharp enough to resolve fine splittings due to the rotational motion and the crystal field interaction, as seen in Figure 2.

(b) Spin−Orbit Transition of I Atom. Figure 3 compares the spin−orbit transition of I atoms in solid *p*-H_2 and in solid *o*-D_2. The concentration of CD_3I in the premixed gas was 4 ppm. The transition at 7655 cm^{-1} is assigned to the spin−orbit transition of iodine atoms isolated in solid *o*-D_2. The transition frequency of iodine atoms in solid *o*-D_2 and that in solid *p*-H_2 are summarized in Table 2. The iodine atom giving rise to the absorption at 7655 cm^{-1} is supposed to be well separated in the solid by photoinduced fragmentation, so there is no perturbation to the spin−orbit transition of the I atom from other impurities.[54] The fine spectral structure seen in the absorption band of I atom in solid *p*-H_2 has been interpreted as the

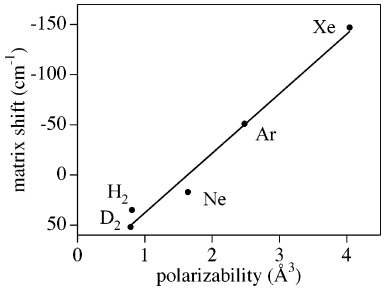

Figure 4. Matrix shift of the $^2P_{1/2} \leftarrow {}^2P_{3/2}$ transition of I atoms in various cryogenic matrices as a function of the dipole polarizability: $\alpha(Xe) = 4.04$ Å^3,[56] $\alpha(Kr) = 2.48$ Å^3,[56] $\alpha(Ar) = 1.64$ Å^3,[56] $\alpha(H_2) = 0.81$ Å^3,[57] and $\alpha(D_2) = 0.79$ Å^3.[57]

hyperfine structure of the I atom ($I = {}^5/_2$ nuclear spin) broadened by the crystal field.[54] The similar doublet structure is barely seen in the spectrum in solid *o*-D_2.

The frequency of the magnetic dipole transition of the iodine atom in solid *o*-D_2 is 52 cm^{-1} higher than that in the gas phase. It has been reported[55] that the transition frequency is also blue-shifted in solid Ar but red-shifted in solid Kr and Xe. The shift must be a result of intermolecular interactions between guest and host matrices. Since interaction in solid hydrogen and in solid rare gas matrices is mainly a dispersion interaction, the shift must be related to the dipole polarizability, α, of a constituent of the host crystals. Figure 4 plots the matrix shifts as a function of the dipole polarizability.[56,57] The matrix shift is almost proportional to the polarizability of crystals. The sign change of the shift indicates that the energy shifts of $^2P_{1/2}$ and $^2P_{3/2}$ states depend on the polarizability; when $\alpha < 2$ Å,^{3} the $^2P_{3/2}$ state is more stabilized than the $^2P_{1/2}$ state, while vice versa when $\alpha > 2$ Å.^{3} The change in the polarizability of H_2 and D_2 is almost negligible (0.81 Å^3 for H_2 and 0.79 Å^3 for D_2),[57] but the shift of the magnetic dipole transition in solid *o*-D_2 (52 cm^{-1}) is clearly larger than that in solid *p*-H_2 (35 cm^{-1}). The larger shift in solid *o*-D_2 must be due to the smaller lattice constant in solid *o*-D_2 (3.6 Å) than in solid *p*-H_2 (3.8 Å).[31] The smaller lattice constant makes the interaction slightly stronger in solid *o*-D_2, which causes the larger shift of transition frequency.

The width of the spin−orbit transition of I atoms is slightly broader in solid *o*-D_2 than in solid *p*-H_2, as seen in Figure 3. The broader width in solid *o*-D_2 could be due to the stronger interaction in solid *o*-D_2 than in solid *p*-H_2 and the quadrupolar interaction of the residual $J = 1$ *p*-D_2 impurities. The width, however, is still sharp enough to resolve splitting due to the hyperfine structure of I atoms.

When the initial concentration of CD_3I in the premixed gas was increased to 50−100 ppm, an additional transition was observed in the magnetic dipole transition of I atoms after UV photolysis. The left panels in Figure 5 show the magnetic dipole transition of I atoms in such samples. In both solid *p*-H_2 and solid *o*-D_2, an additional doublet was observed at slightly higher frequency of the magnetic dipole transition of free I atoms, whose transition frequencies are listed in Table 2. In such samples, the absorption corresponding to deuterated ethane (C_2D_6) was always observed at 2081 cm^{-1}, as shown in the right panels of Figure 5. Since ethane molecules are produced in the cluster of CD_3I trapped in solid hydrogen, the additional doublet at 7675 cm^{-1} in solid *o*-D_2 and 7661 cm^{-1} in solid *p*-H_2 must be due to the magnetic dipole transition of I atoms in such clusters of guest molecules. Perturbation from nearby impurity molecules, plausibly C_2D_6 or CD_3I in this case, shifts the magnetic dipole transition by about 20 cm^{-1} toward blue.[54] We did not observe any change in the intensity of such an additional doublet for a few days as well as upon annealing, which indicates that the I atoms in such complexes are fairly stable. A similar shift of the magnetic dipole transition of I atoms in solid *p*-H_2 has been observed for other systems.[58]

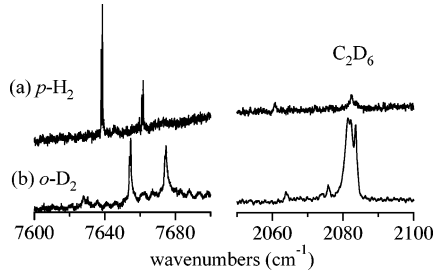

Figure 5. (a) An FTIR spectrum of the spin−orbit transition of I atoms in solid *p*-H_2. (b) An FTIR spectrum of the spin−orbit transition of I atoms in solid *o*-D_2. The concentration of CD_3I in the premixed gas was 50 ppm. The right panels shows the corresponding spectral region of the absorption of CD_3I and C_2D_6.

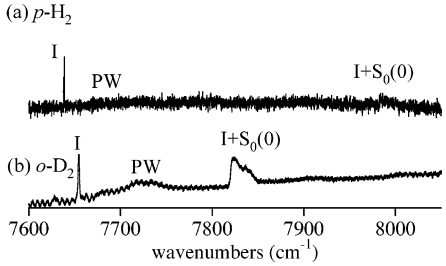

Figure 6. The $^2P_{1/2} \leftarrow {}^2P_{3/2}$ transition of I atoms in solid hydrogen in the spectral range of 7600−8400 cm^{-1}: (a) in solid *p*-H_2 and (b) in solid *o*-D_2. I: the transition of isolated I atoms. PW: phonon side band of the spin−orbit transition of I atoms. I + $S_0(0)$: the simultaneous transitions of an I atom and $S_0(0)$ transition of solid hydrogen.

(c) Electron−Phonon and Electron−Roton Couplings. Depending on the magnitude of the electron phonon coupling, electronic transitions are often accompanied by phonon side bands at higher frequency.[59] Such phonon side bands for the magnetic dipole transition of I atoms have been reported in solid Ar, Kr, and Xe,[55] indicating the large electron−phonon coupling. In solids of *o*-D_2 and *p*-H_2, similar phonon side bands were observed, as indicated by PW in Figure 6, which appear 68 and 74 cm^{-1}, respectively, higher than the transition of the isolated I atom in solid *o*-D_2 and *p*-H_2. The intensity of the phonon side band in solid *o*-D_2 is strong enough to observe clearly, but that in solid *p*-H_2 is barely seen. Compared with other rare gas matrices,[55] the PW in solid *o*-D_2 and *p*-H_2 are extremely weak. The weak phonon side band in solid hydrogen indicates weak coupling between the spin−orbit transition and the phonon modes, even though the lattice vibrations are the lowest excitation mode in the solids. The weak absorption of phonon side bands must reflect the weak intermolecular interaction of $J = 0$ hydrogen. The interaction of $J = 0$ *o*-D_2 must be slightly stronger than that of $J = 0$ *p*-H_2 to cause stronger PW in solid *o*-D_2.

In solid *o*-D_2, an additional broad band is observed around 7838 cm^{-1}, as seen in Figure 6. This band is blue-shifted by 180 cm^{-1} from the transition of the isolated iodine atom at 7654 cm^{-1}. Since the shift is nearly the same as the frequency of the $S_0(0)$ transition ($J = 2 \leftarrow J = 0$) of *o*-D_2 molecules at 176 cm^{-1},[33] the band is attributed to the simultaneous transition of the magnetic dipole transition of the iodine atom and the pure rotational transition of *o*-D_2 molecules. Here, we denote the transition as I + $S_0(0)$. The corresponding transition is also seen at 7994 cm^{-1} in solid *p*-H_2, where the shift from the transition

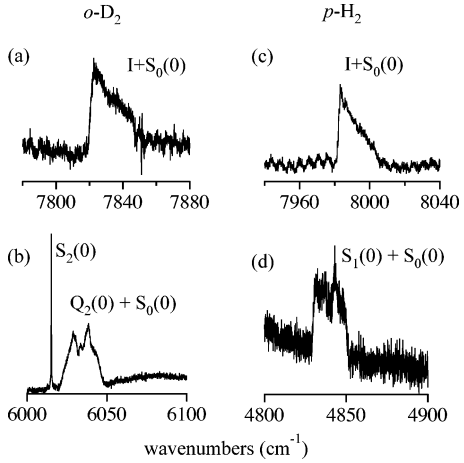

Figure 7. (a) The I + $S_0(0)$ simultaneous transition of I atoms in solid *o*-D_2. (b) The $Q_2(0)$ + $S_0(0)$ simultaneous transition in solid *o*-D_2. (c) The I + $S_0(0)$ simultaneous transition of I atoms in solid *p*-H_2. (d) The $S_1(0)$ + $S_0(0)$ simultaneous transition in solid *p*-H_2.

of isolated iodine atom is 355 cm^{-1}, which is in good agreement with the transition frequency of the $S_0(0)$ transition of *p*-H_2 at 356 cm^{-1}.[30,33]

The full bandwidth of the I + $S_0(0)$ transition measured at the bottom of the broad band is about 30 cm^{-1}, which is an order of magnitude broader than the line width of the spin−orbit transition of I atoms isolated in solid *o*-D_2 and *p*-H_2. The broad bandwidth of the simultaneous transition can be interpreted in terms of the $J = 2$ rotational manifold. It is known that the $J = 2$ level of *o*-D_2/*p*-H_2 molecules builds up a band structure in solid *o*-D_2/*p*-H_2 called the roton band.[30] For a single transition, $J = 2$ rotational excitations are only to the $k = 0$ level of the roton band due to the conservation of the crystal momentum (k), namely the $\Delta k = 0$ selection rule, where only three states in the $J = 2$ band are optically allowed.[30] When the roton band is excited simultaneously with other excitation, such as vibrational or electronic excitation in an impurity molecule inside the solid, the $\Delta k = 0$ selection rule can be achieved in a way that the roton carries a momentum with $+k$ and the other excitation with $-k$. As a result, all states in the roton band become optically allowed in simultaneous transitions. Thus, the bandwidth of the I + $S_0(0)$ transition must reflect the bandwidth of the $J = 2$ roton band, whose estimated bandwidth is 31.0 cm^{-1} in solid *o*-D_2 and 25.0 cm^{-1} in solid *p*-H_2.[30] Figure 7 compares the I + $S_0(0)$ transitions in solid *o*-D_2 and solid *p*-H_2 with simultaneous transitions of solid hydrogen itself. The sharp absorption at 6015 cm^{-1} in panel b of Figure 7 is the $S_2(0)$ transition of solid *o*-D_2, while the broad band in the range of 6020−6050 cm^{-1} is the $Q_2(0)$ + $S_0(0)$ simultaneous transition. The $S_2(0)$ transition is a single transition, so it appears as a sharp transition as a result of the $\Delta k = 0$ selection rule. On the other hand, the $Q_2(0)$ + $S_0(0)$ simultaneous transition shows a width of about 30 cm^{-1}, corresponding to the width of the $S_0(0)$ roton band of solid *o*-D_2. The width of the $Q_2(0)$ + $S_0(0)$ simultaneous transition is about the same as that of the I + $S_0(0)$ transition in solid *o*-D_2, as shown in the panel a of Figure 7. Panels c and d compare the simultaneous transitions of I + $S_0(0)$ and $S_1(0)$ + $S_0(0)$ in solid *p*-H_2. Again, the width is roughly 25 cm^{-1} in both transitions, corresponding to the width of the $S_0(0)$ roton band of solid *p*-H_2.

The I + $S_0(0)$ simultaneous transition is stronger than the phonon sideband, which indicates stronger electron−roton coupling than the electron−phonon coupling. The phonon sideband is a result of the interaction between the $J = 0$ hydrogen and the magnetic transition of I atoms. Since there are no permanent multipole moments in the $J = 0$ hydrogen, interaction between the $J = 0$ hydrogen and the magnetic transition of I atoms is expected to be small. On the other hand, the I + $S_0(0)$ simultaneous transition is a result of the interaction between the $J = 2$ hydrogen and the magnetic transition of I atoms. The electric quadrupole moment of the $J = 2$ hydrogen could interact with the electric field gradient generated by the finite electric distribution of the 5p orbital of iodine atoms. Thus, the electron−roton coupling is expected to be stronger than electron−phonon coupling in solid hydrogen. So far, many double transitions such as roton + roton, roton + vibron, vibron + libron, and vibron + phonon in pure solid hydrogens have been observed,[30,60] while few siumltaneous transitions of doped molecules/atoms and hydrogen molecules have been reported.[5,61] Recently, it has been reported that other halogen atoms in solid hydrogen show similar transitions due to the electron−roton coupling, whose intensities are significantly different for different halogen atoms.[5,61] The analysis of the intensity of these simultaneous transitions of dopant molecules/atoms and hydrogen molecules will give us more information on the interaction between these two species.

(d) Tunneling Reaction between CD_3 and D_2. In previous studies, we found that methyl radicals of CD_3 produced in solid *p*-H_2 react with a surrounding H_2 molecule via a quantum tunneling effect. It is worthwhile investigating the isotope effect on the tunneling reaction of $CD_3 + X_2 \rightarrow CD_3X + X$ (X = H or D). The barrier of the reaction between a methyl radical and a hydrogem molecule is known to be about 11 kcal $mol^{-1} \sim$ 3850 $cm^{-1} \sim$ 5500 K.[62] Therefore, if the reaction occurs at 4 K, it must be due to the pure tunneling process. The tunneling reaction rate of CD_3 in solid *p*-H_2 has been determined to be 3.3×10^{-6} s^{-1}.[15] Since the tunneling particle in the reaction of $CD_3 + D_2 \rightarrow CD_4 + D$ is a D atom, the tunneling rate of this reaction is expected to be roughly four times slower than that in the H_2 system. The estimated tunneling rate is 8.3×10^{-7} s^{-1}, corresponding to about 7% decrease of the absorption of CD_3 after 1 day. However, no decrease of the absorption of CD_3 nor any trace of an absorption of CD_4 was observed in solid *o*-D_2 after 3 days. We estimate the upper limit of the tunneling rate of the reaction $CD_3 + D_2 \rightarrow CD_4 + D$ to be 1×10^{-8} s^{-1} at most.

The reaction enthalpy including zero point vibrational energies (ZPVEs) of the reactants and products must be negative, otherwise the tunneling reaction cannot proceed at any temperature. In the case of the reaction $CD_3 + D_2 \rightarrow CD_4 + D$, the ZPVE of the product is 2.52 kcal mol^{-1} larger than that of the reactants, which is obtained by using ZPVE(D_2) = 4.45 kcal mol^{-1}, ZPVE(CD_3) = 13.8 kcal mol^{-1}, and ZPVE(CD_4) = 20.77 kcal mol^{-1}.[63] The electronic energy of the reactants is calculated to be higher by 2.62−3.15 kcal mol^{-1} than that of the products.[14] Therefore, it is expected that the reactants are slightly unstable with respect to the products, suggesting that the tunneling reaction of $CD_3 + D_2 \rightarrow CD_4 + D$ could occur in solid *o*-D_2. However, the estimated upper limit of the tunneling rate of 1×10^{-8} s^{-1} is almost 2 orders of magnitude smaller than that of $CD_3 + H_2 \rightarrow CD_3H + H$. Note that in the case of $CD_3 + H_2 \rightarrow CD_3H + H$, the ZPVE of the product is also 2.52 kcal mol^{-1} larger than that of the reactants. Therefore, the difference in the total energies between the $CD_3 + D_2 \rightarrow CD_4 + D$ reaction system and $CD_3 + H_2 \rightarrow CD_3H + H$ system is almost exactly the same. Nevertheless, we did not observe any tunneling reaction of $CD_3 + D_2 \rightarrow CD_4 + D$ within our experimental time scale. The difference between $CD_3 + H_2 \rightarrow$

$CD_3H + H$ and $CD_3 + D_2 \rightarrow CD_4 + D$ must be due to the isotope effect on the entire potential surface. A quantum chemical calculation with good quality is needed to understand the observed difference.

Conclusions

Here, we showed that solid *o*-D_2 is another excellent matrix for high-resolution spectroscopy of dopant molecules as well as for photochemistry and tunneling reactions. We have shown that methyl radicals rotate almost freely in solid *o*-D_2, as in the case of solid *p*-H_2. The linewidths of rovibrational and electronic transitions in solid *o*-D_2 are slightly broader than those in solid *p*-H_2 due to the larger concentration of $J = 1$ impurities in solid *o*-D_2 than in solid *p*-H_2, but the widths are still narrow enough to resolve fine structures such as hyperfine splitting in the spin−orbit transition of I atoms. As for the in situ photolysis, the cage effect in solid *o*-D_2 is weak enough to allow photodissociation of molecules in the solid as in *p*-H_2. We found that the tunneling reaction of $CD_3 + D_2 \rightarrow CD_4 + D$ did not occur within our experimental time scale, which is in contrast to the relatively fast tunneling reaction in the $CD_3 + H_2 \rightarrow CD_3H + H$ reaction system. Comparison of tunneling reactions in solid *o*-D_2 and in solid *p*-H_2 would give us more detailed information on the quantum tunneling effect in chemical reactions, which is difficult to obtain by other experimental techniques.

Acknowledgment. This work was supported by Grant-in-Aid for Scientific Research of the Ministry of Education, Science, Culture, and Sports of Japan, and by the Natural Sciences and Engineering Research Council (NSERC) Discovery Grant in Canada.

References and Notes

(1) Momose, T.; Shida, T. *Bull. Chem. Soc. Jpn.* **1998**, *71*, 1.
(2) Momose, T.; Hoshina, H.; Fushitani, M.; Katsuki, H. *Vib. Spectrosc.* **2004**, *34*, 95.
(3) Momose, T.; Fushitani, M.; Hoshina, H. *Int. Rev. Phys. Chem.* **2005**, *24*, 533.
(4) Fajardo, M. E.; Tam, S. *J. Chem. Phys.* **1998**, *108*, 4237.
(5) Anderson, D. T.; Hinde, R. J.; Tam, S.; Fajardo, M. E. *J. Chem. Phys.* **2002**, *116*, 594.
(6) Yoshioka, K.; Raston, P.; Anderson, D. T. *Int. Rev. Phys. Chem.* **2006**, *25*, 469.
(7) Wu, Y.-J.; Yang, X.; Lee, Y.-P. *J. Chem. Phys.* **2004**, *120*, 1168.
(8) Lee, Y. -P.; Wu, Y-J.; Lees, R. M.; Xu, L.-H.; Hougen, J. T. *Science* **2006**, *311*, 365.
(9) Scoles, G. *Atomic and Molecular Beam Methods*, Oxford University Press: New York, 1988; Vol. 1, p 2.
(10) Goyal, S.; Schutt, D. L.; Scoles, G. *Phys. Rev. Lett.* **1992**, *69*, 933.
(11) Toennies, J. P.; Vilesov, A. F. *Annu. Rev. Phys. Chem.* **1998**, *49*, 1.
(12) Toennies, J. P.; Vilesov, A. F. *Angew. Chem., Int. Ed.* **2004**, *43*, 2622.
(13) Stienkemeier, F.; Lehmann, K. K. *J. Phys. B: At. Mol. Opt. Phys.* **2006**, *39*, R127.
(14) Momose, T.; Hoshina, H.; Sogoshi, N.; Katsuki, H.; Wakabayashi, T.; Shida, T. *J. Chem. Phys.* **1998**, *108*, 7334.
(15) Hoshina, H.; Fushitani, M.; Momose, T.; Shida, T. *J. Chem. Phys.* **2004**, *120*, 3706.
(16) Momose, T.; Miki, M.; Uchida, M.; Shimizu, T.; Yoshizawa, I.; Shida, T. *J. Chem. Phys.* **1995**, *103*, 1400.
(17) Fushitani, M.; Sogoshi, N.; Wakabayashi, T.; Momose, T.; Shida, T. *J. Chem. Phys.* **1998**, *109*, 6346.
(18) Fushitani, M.; Shida, T.; Momose, T.; Räsänen, M. *J. Phys. Chem. A*, **2000**, *104*, 3635.
(19) Mador, I. L. *J. Chem. Phys.* **1954**, *22*, 1617.
(20) Pimentel, G. C. *Formation and Trapping of Free Radicals;* Bass, A. M., Broida, H. P., Eds.; Academic Press: New York, 1960; Chapter 4, p 69.
(21) Andrews, L.; Pimentel, G. C. *J. Chem. Phys.* **1967**, *47*, 3637.
(22) Brus, L. E.; Bondybey, V. E. *J. Chem. Phys.* **1976**, *65*, 71.
(23) Raston, P. L.; Anderson, D. T. *J. Chem. Phys.* **2007**, *126*, 021106.
(24) Kumada, T.; Sakakibara, M.; Nagasaka, T.; Fukuta, H.; Kumagai, J.; Miyazaki, T. *J. Chem. Phys.* **2002**, *116*, 1109.
(25) Fushitani, M.; Momose, T. *Low Temp. Phys.* **2003**, *29*, 740.
(26) Raston, P. L.; Anderson, D. T. *Phys. Chem. Chem. Phys.* **2006**, *8*, 3124.
(27) Fushitani, M.; Momose, T. *J. Chem. Phys.* **2002**, *116*, 10739.
(28) Miyamoto, Y.; Tsubouchi, M.; Momose, T. In preparation.
(29) Silvera, I. F. *Rev. Mod. Phys.* **1980**, *52*, 393.
(30) van Kranendonk, J. *Solid Hydrogen. Theory of the Properties of Solid H_2, HD, and D_2,* Plenum: New York 1983.
(31) Souers, P. C. *Hydrogen Properties for Fusion Energy;* University of California Press: Berkeley, CA, 1986.
(32) Friedmann, H. *Adv. Chem. Phys.* **1962**, *4*, 280.
(33) Silvera, I. F.; Wijngaarden, R. J. *Phys. Rev. Lett.* **1981**, *47*, 39.
(34) Chan, M.-C.; Oka, T. *J. Chem. Phys.* **1990**, *93*, 979.
(35) Meyer, H. *Physica* **1994**, *B197*, 13.
(36) Katsuki, H.; Fushitani, M.; Momose, T. *Low Temp. Phys.* **2003**, *29*, 832.
(37) Kozioziemski, B. J.; Collins, G. W. *Phys. Rev.* **2003**, *B67*, 174101.
(38) Andrews, L.; Wang, X. *J. Chem. Phys.* **2004**, *121*, 4724.
(39) Stenum, B.; Schou, J.; Sørensen, H.; Gürtler, P. *J. Chem. Phys.* **1993**, *98*, 126.
(40) Danilychev, A. V.; Bondybey, V. E.; Apkarian, V. A.; Tanaka, S.; Kajihara, H.; Koda, S. *J. Chem. Phys.* **1995**, *103*, 4292.
(41) Vigliotti, F.; Cavina, A. Ch. Bressler, Lang, B.; Chergui, M. *J. Chem. Phys.* **2002**, *116*, 4542.
(42) Kumada, T. *J. Chem. Phys.* **2002**, *117*, 10133.
(43) Tam, S.; Fajardo, M. E. *Rev. Sci. Instrum.* **1999**, *70*, 1926.
(44) Fawzy, W. M.; Sears, T. J.; Davies, P. B. *J. Chem. Phys.* **1990**, *92*, 7021.
(45) He, Y.; Quack, M.; Ranz, R.; Seyfang, G. *Chem. Phys. Lett.* **1993**, *215*, 228.
(46) Tam, S.; Fajardo, M. E.; Katsuki, H.; Hoshina, H.; Wakabayashi, T.; Momose, T. *J. Chem. Phys.* **1999**, *111*, 4191.
(47) Momose, T. *J. Chem. Phys.* **1997**, *107*, 7695.
(48) Hoshina, H.; Fushitani, M.; Momose, T. In preparation.
(49) Herzberg, G. *Molecular Spectra and Molecular Structure II, Infrared and Raman Spectra of Polyatomic Molecules*; Krieger Publishing Co.: Malabar, FL, 1991.
(50) Wigner, E. P. *Group Theory;* Academic Press: New York, 1959.
(51) Frye, J. M.; Sears, T. J.; Leithner, D. *J. Chem. Phys.* **1988**, *88*, 5300.
(52) Manz, J. *J. Am. Chem. Soc.* **1980**, *102*, 1801.
(53) Weliky, D. P.; Byers, T. J.; Kerr, K. E.; Momose, T.; Dickson, R. M.; Oka, T. *Appl. Phys. B* **1994**, *59*, 265.
(54) Fushitani, M.; Momose, T.; Shida, T. *Chem. Phys. Lett.* **2002**, *356*, 375.
(55) Pettersson, M.; Nieminen, J. *Chem. Phys. Lett.* **1998**, *283*, 1.
(56) Miller. T. M.; Bederson, B. *Adv. Atm. Mol. Phys.* **1977**, *13*, 1.
(57) Rychlewski, J. *J. Chem. Phys.* **1983**, *78*, 7252.
(58) In ref 54, we have assigned the additional doublet to the magnetic dipole transition of an I atom loosely complexed with a methyl radical. The present observation indicates that it has to be reassigned to the magnetic dipole transition of an I atom complexed with other stable guest molecules such as CD_3I or C_2D_6.
(59) Rebane, K. *Impurity Spectra of Solids;* Plenum Press: New York, 1970.
(60) Oka, T. *Annu. Rev. Phys. Chem.* **1993**, *44*, 299.
(61) Hinde, R. J.; Anderson, D. T.; Tam, S.; Fajardo, M. E. *Chem. Phys. Lett.* **2002**, *356*, 355.
(62) Kraka, E.; Gauss, J.; Cremer, D. *J. Chem. Phys.* **1993**, *99*, 5306.
(63) Schatz, G. C.; Wagner, A. F.; Dunning, T. H., Jr. *J. Phys. Chem.* **1984**, *88*, 221.